Meso-scale site-bond model for elasticity: theory and calibration

M. Zhang*[1], C. N. Morrison[1,2] and A. P. Jivkov[1]

A meso-scale site-bond model is proposed to simulate the macroscopic elastic properties of isotropic materials. The microstructure of solids is represented by an assembly of truncated octahedral cells with sites at the cell centres and bonds linking the nearest neighbouring sites. Based on the equivalence of strain energy stored in a unit cell to strain energy stored in a continuum of identical volume, the normal and shear stiffness coefficients of bonds are derived from the given macroscopic elastic constants: Young's modulus and Poisson's ratio. To validate the obtained spring constants, benchmark tests including uniaxial tension and plane strain are performed. The simulated macroscopic elastic constants are in excellent agreement with the theoretical values. As a result, the proposed site-bond model can be used to simulate the macroscopic elastic behaviour of solids with Poisson's ratios in the range from −1 up to 1/2.

Keywords: Site-bond model, Elasticity, Lattice spring, Discrete−continuum equivalence, Isotropy

Introduction

The classical homogeneous elasticity is widely used to describe the macroscopic linear mechanical behaviour of most materials, even though they are actually heterogeneous from a microscopic point of view. However, the mechanical response of heterogeneous quasi-brittle materials, such as concrete, rock, graphite or ceramics, cannot be modelled realistically without explicit considerations of their underlying microstructures. This requires numerical approaches which are able to account for not only the elastic stage, but also the initiation, growth, interaction and coalescence of micro-cracks. The discrete lattice approach, usually called the meso-scale approach, shows potential to meet this requirement.[1] In lattice models,[1–10] the microstructures of materials are represented by an assemblage of unit cells or particles. The lattice sites are placed at the centres of the cells. The deformation of the represented continuum arises from the interactions between the lattice sites. The neighbouring cells are linked through interface bonds, which can be represented by lattice beam elements or lattice springs. Compared to the continuum finite element modelling, lattice models have been shown to be more suitable for fracture simulation because of their discrete nature.

The lattice models have been successfully applied to the modelling of quasi-brittle materials. The macroscopic stress–strain curve for concrete is obtained by using a lattice beam model based on a two-dimensional regular lattice with hexagonal unit cells.[2,3] However, this lattice cannot be used for isotropic elastic materials with Poisson's ratio larger than 1/3 in plane stress and 1/4 in plane strain.[4] Based on the simplest regular lattice with cubic cells, a three-dimensional (3D) lattice beam model has been proposed by Schlangen[5] to simulate the crack development in concrete. It has been shown that this lattice is only suitable for materials with zero Poisson's ratio.[6] With respect to lattice spring models, Wang and Mora[7] developed two 3D lattices using face-centred cubic and hexagonal closely-packed arrangements. Each pair of sites in the lattice network is connected by spring. It was found that only isotropic elastic material with Poisson's ratio of zero can be represented by these lattices, which is the same as cubic lattices. To overcome these limitations, a site-bond based on a bi-regular lattice of truncated octahedron cells has been recently proposed by Jivkov and Yates[1] for meso-scale modelling of solids. The bonds of the site-bond assembly are modelled with structural beam elements. It has been demonstrated that this site-bond model is able to represent isotropic elastic materials with Poisson's ratios up to 1/2.

The main purpose of this work is to reformulate the site-bond assembly presented in Ref. 1 by modelling the bonds with two types of elastic springs instead of structural beam elements to further study the capability of this lattice arrangement for the macroscopic elastic behaviour of practical interest. The stiffness coefficients of springs are analytically determined by equating the strain energy stored in the discrete and continuum cell. The derived spring constants are validated through numerical analyses.

Site-bond model

In the site-bond model, the microstructure of a real material is represented by tessellating the space into truncated octahedral cells, as shown in Fig. 1*a*. The

[1]Modelling & Simulation Centre and Research Centre for Radwaste & Decommissioning, The University of Manchester, Manchester M13 9PL, UK
[2]Nuclear FiRST Doctoral Training Centre, The University of Manchester, Manchester M13 9PL, UK

*Corresponding author, email mingzhong.zhang@manchester.ac.uk

Received 15 September 2013; accepted 12 December 2013
DOI 10.1179/1432891714Z.000000000537

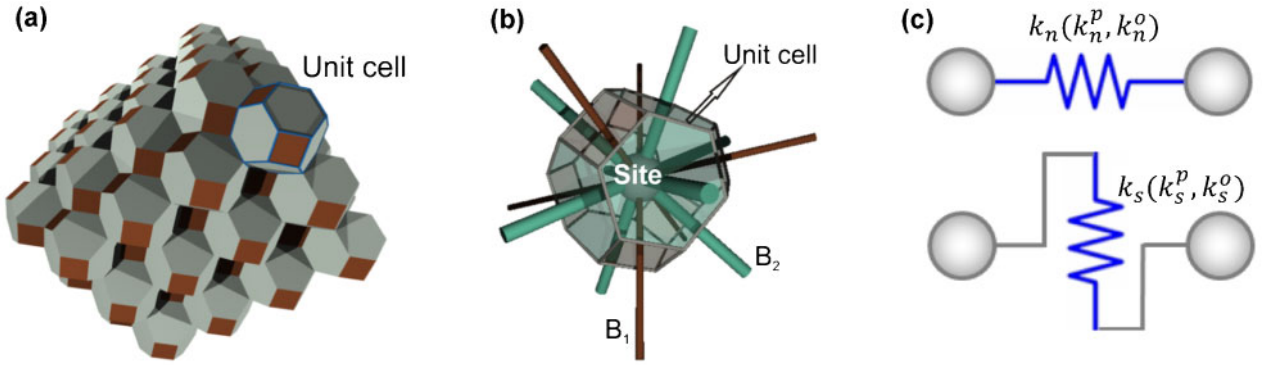

1 Cellular lattice: *a* site-bond assembly; *b* unit cell with bonds; *c* normal and shear springs

truncated octahedron was found to be the best choice for a regular representation of real materials compared to the cube, the regular hexagonal prism or the rhombic dodecahedron.[1,6] Each cell has six equal square faces and eight equal hexagonal faces. The cell centre is considered as a site, which is connected with its neighbouring sites by 14 bonds, six bonds B_1 in principal directions through square faces and eight bonds B_2 in octahedral directions through hexagonal faces, as illustrated in Fig. 1*b*.

In this study, the bonds are modelled with elastic springs. The sites have six independent degrees of freedom: three translational and three rotational. In principle, each bond should contain six springs: one normal, two shear, one twisting, and two bending springs in order to resist the relative displacement and relative rotations between the two adjacent cells. However, it was presented that the twisting stiffness k_t and bending stiffness k_b are related to the shear stiffness k_s and normal stiffness k_n, respectively, with the contribution of k_t and k_b to the macroscopic elasticity effectively negligible in comparison to k_s and k_n.[7] Therefore, only the normal and shear springs in principal and octahedral directions are considered herein, as shown in Fig. 1*c*.

Derivation of spring constants for site-bond model

In this section, the spring constants are derived from the macroscopic elastic parameters by equating the strain energy stored in a unit cell U_{cell} to the associated strain energy in the equivalent continuum system U_{cont}

$$U_{\text{cell}} = U_{\text{cont}} \tag{1}$$

The strain energy of the continuum system is given by

$$U_{\text{cont}} = \frac{1}{2}\int_{\text{V}} \sigma\varepsilon \text{d}V = \frac{1}{2}C_{\text{ijkl}}\varepsilon_{\text{ij}}\varepsilon_{\text{kl}}\text{V} \tag{2}$$

where C represents the stiffness tensor of the material, ε is the strain field and V is the system volume. The strain energy stored in a unit cell can be expressed as a sum of the strain energies stored in each internal bond U_{b}

$$U_{\text{cell}} = \sum_{\text{b}} U_{\text{b}} = \frac{1}{4}\sum_{\text{b}}^{\text{N}_\text{b}} \left(k_{\text{n}}^{(\text{b})} u_{\text{n}}^{(\text{b})} u_{\text{n}}^{(\text{b})} + k_{\text{s}}^{(\text{b})} u_{\text{s}}^{(\text{b})} u_{\text{s}}^{(\text{b})}\right) \tag{3}$$

in which $u_{\text{n}}^{(\text{b})}$ and $u_{\text{s}}^{(\text{b})}$ stand for the relative displacements in the normal direction and transverse direction of the bond, respectively. Let us assume that the bond b links two sites A and B, then the relative normal and shear displacements in the 3D global system $X_1X_2X_3$ can be written as

$$u_{\text{n}}^{(\text{b})} = \Delta u_{\text{i}}^{(\text{b})} \xi_{\text{i}}^{(\text{b})} \tag{4}$$

$$u_{\text{s}}^{(\text{b})} = \Delta u_{\text{i}}^{(\text{b})} - u_{\text{n}}^{(\text{b})} \xi_{\text{i}}^{(\text{b})} \tag{5}$$

in which

$$\Delta u_{\text{i}}^{(\text{b})} = \varepsilon_{\text{ij}} \Delta x_{\text{j}} = \varepsilon_{\text{ij}}(x_{\text{jB}} - x_{\text{jA}}) \tag{6}$$

The direction vector of the bond $\xi_{\text{i}}^{(\text{b})}$ is given as

$$\xi_{\text{i}}^{(\text{b})} = \frac{(x_{\text{iB}} - x_{\text{iA}})}{L_{\text{AB}}} \tag{7}$$

where x_{iA} and x_{iB} are the positions of the sites, L_{AB} is the length of the bond. By substituting equations (4)–(7) into equation (3) and performing tensor and vector manipulations, equation (3) can be expressed as

$$U_{\text{cell}} = \frac{1}{4}\sum_{\text{b}}^{\text{N}_\text{b}} (L^{(\text{b})})^2 \left[k_{\text{n}}^{(\text{b})} \xi_{\text{i}}^{(\text{b})} \varepsilon_{\text{ij}} \xi_{\text{j}}^{(\text{b})} \xi_{\text{k}}^{(\text{b})} \varepsilon_{\text{kl}} \xi_{\text{l}}^{(\text{b})} + k_{\text{s}}^{(\text{b})} \left(\varepsilon_{\text{kl}} \xi_{\text{l}}^{(\text{b})} - \xi_{\text{i}}^{(\text{b})} \varepsilon_{\text{ij}} \xi_{\text{j}}^{(\text{b})} \xi_{\text{k}}^{(\text{b})}\right)\left(\varepsilon_{\text{km}} \xi_{\text{m}}^{(\text{b})} - \xi_{\text{n}}^{(\text{b})} \varepsilon_{\text{nm}} \xi_{\text{m}}^{(\text{b})} \xi_{\text{k}}^{(\text{b})}\right)\right] \tag{8}$$

in which $L^{(\text{b})}$ is the length of a bond b. Then by equating the total strain energy stored per unit volume V, the strain energy density ρ_{cont}, to that in the unit cell $\rho_{\text{cell}} = U_{\text{cell}}/V$ and by using Cauchy's formula,[8–10] the stress tensor of the continuum system can be obtained as

$$\sigma_{\text{ij}} = \frac{\partial \rho_{\text{cont}}}{\partial \varepsilon_{\text{ij}}} = \frac{1}{2V}\sum_{\text{b}}^{\text{N}_\text{b}} (L^{(\text{b})})^2 \left[k_{\text{s}}^{(\text{b})} \varepsilon_{\text{il}} \xi_{\text{l}}^{(\text{b})} \xi_{\text{j}}^{(\text{b})} + \left(k_{\text{n}}^{(\text{b})} - k_{\text{s}}^{(\text{b})}\right) \varepsilon_{\text{kl}} \xi_{\text{i}}^{(\text{b})} \xi_{\text{j}}^{(\text{b})} \xi_{\text{k}}^{(\text{b})} \xi_{\text{l}}^{(\text{b})}\right] \tag{9}$$

Finally, the elastic stiffness tensor can be given as

$$C_{\text{ijkl}} = \frac{\partial \sigma_{\text{ij}}}{\partial \varepsilon_{\text{kl}}} = \frac{1}{2V}\sum_{\text{b}}^{\text{N}_\text{b}} (L^{(\text{b})})^2 \left[k_{\text{s}}^{(\text{b})} \delta_{\text{ik}} \xi_{\text{j}}^{(\text{b})} \xi_{\text{l}}^{(\text{b})} + \left(k_{\text{n}}^{(\text{b})} - k_{\text{s}}^{(\text{b})}\right) \xi_{\text{i}}^{(\text{b})} \xi_{\text{j}}^{(\text{b})} \xi_{\text{k}}^{(\text{b})} \xi_{\text{l}}^{(\text{b})}\right] \tag{10}$$

where δ_{ik} is the Kroecker's delta.

Considering the site-bond assembly shown in Fig. 1 and assuming that the unit cell size in the principal directions is L, the lengths of bonds B_1 and B_2 are L and $3^{1/2}L/2$, respectively. The volume of the unit cell V is $L^3/2$. For each bond, $k_{\text{n}}^{(\text{b})}$ and $k_{\text{s}}^{(\text{b})}$ are the normal and shear spring constants for bonds B_1 and B_2, which are denoted as k_{n}^{p} and k_{s}^{p}, k_{n}^{o} and k_{s}^{o}, respectively in the following

sections. The direction vectors of bonds B_1 and B_2 are given in Table 1.

Hence, by using equation (10) and assuming the two shearing spring stiffness coefficients are equal within each bond type but different between the two bond types, B_1 and B_2, we get the components of the stiffness tensor

$$C_{1111} = \frac{2}{3L}\left(3k_{\mathrm{n}}^{\mathrm{p}} + k_{\mathrm{n}}^{\mathrm{o}} + 2k_{\mathrm{s}}^{\mathrm{o}}\right) = C_{2222} = C_{3333} \tag{11}$$

$$C_{1122} = \frac{2}{3L}\left(k_{\mathrm{n}}^{\mathrm{o}} - k_{\mathrm{s}}^{\mathrm{o}}\right) = C_{1133} = C_{2233} = C_{2211} = C_{3311} = C_{3322} \tag{12}$$

$$C_{1212} = \frac{2}{3L}\left(3k_{\mathrm{s}}^{\mathrm{p}} + k_{\mathrm{n}}^{\mathrm{o}} + 2k_{\mathrm{s}}^{\mathrm{o}}\right) = C_{1313} = C_{2323} = C_{2121} = C_{3131} = C_{3232} \tag{13}$$

$$\text{Other } C_{\mathrm{ijkl}} = 0 \tag{14}$$

It can be seen from equations (11)–(14) that there are only three independent elastic constants. This indicates that the site-bond assembly generates macroscopic cubic elasticity. With the Voigt notation, which is the standard mapping for tensor indices, the spring constants can be expressed as

$$k_{\mathrm{n}}^{\mathrm{p}} = -k_{\mathrm{n}}^{\mathrm{o}} + \frac{L}{2}(C_{11} + 2C_{12}) \tag{15}$$

$$k_{\mathrm{s}}^{\mathrm{p}} = -k_{\mathrm{n}}^{\mathrm{o}} + \frac{L}{2}(2C_{12} + C_{44}) \tag{16}$$

$$k_{\mathrm{s}}^{\mathrm{o}} = k_{\mathrm{n}}^{\mathrm{o}} - \frac{3L}{2}C_{12} \tag{17}$$

Meanwhile, from equations (11)–(14), we find that only when $3k_{\mathrm{n}}^{\mathrm{p}} - 6k_{\mathrm{s}}^{\mathrm{p}} - 2k_{\mathrm{n}}^{\mathrm{o}} - k_{\mathrm{s}}^{\mathrm{o}} = 0$, the site-bond assembly is able to yield macroscopic isotropic elasticity. For isotropic materials, Hooke's law in terms of matrix form can be written as

$$\begin{bmatrix}\sigma_1\\ \sigma_2\\ \sigma_3\\ \sigma_4\\ \sigma_5\\ \sigma_6\end{bmatrix} = \begin{bmatrix} C_{11} & C_{12} & C_{12} & 0 & 0 & 0\\ C_{21} & C_{11} & C_{12} & 0 & 0 & 0\\ C_{21} & C_{21} & C_{11} & 0 & 0 & 0\\ 0 & 0 & 0 & C_{44} & 0 & 0\\ 0 & 0 & 0 & 0 & C_{55} & 0\\ 0 & 0 & 0 & 0 & 0 & C_{66}\end{bmatrix}\begin{bmatrix}\varepsilon_1\\ \varepsilon_2\\ \varepsilon_3\\ 2\varepsilon_4\\ 2\varepsilon_5\\ 2\varepsilon_6\end{bmatrix}$$

Table 1 Direction vectors of bonds B_1 and B_2 in the site-bond assembly

Bond type	Bond no. *b*	$\xi_{\mathrm{i}}^{(\mathrm{b})}$
B_1	1	(1, 0, 0)
	2	(0, 1, 0)
	3	(0, 0, 1)
	4	(−1, 0, 0)
	5	(0, −1, 0)
	6	(0, 0, −1)
B_2	7	$(1/3^{1/2}, -1/3^{1/2}, -1/3^{1/2})$
	8	$(1/3^{1/2}, 1/3^{1/2}, -1/3^{1/2})$
	9	$(1/3^{1/2}, -1/3^{1/2}, 1/3^{1/2})$
	10	$(1/3^{1/2}, 1/3^{1/2}, 1/3^{1/2})$
	11	$(-1/3^{1/2}, 1/3^{1/2}, 1/3^{1/2})$
	12	$(-1/3^{1/2}, -1/3^{1/2}, 1/3^{1/2})$
	13	$(-1/3^{1/2}, 1/3^{1/2}, -1/3^{1/2})$
	14	$(-1/3^{1/2}, -1/3^{1/2}, -1/3^{1/2})$

$$= \frac{E}{(1+\nu)(1-2\nu)}\begin{bmatrix} 1-\nu & \nu & \nu & 0 & 0 & 0\\ \nu & 1-\nu & \nu & 0 & 0 & 0\\ \nu & \nu & 1-\nu & 0 & 0 & 0\\ 0 & 0 & 0 & (1-2\nu)/2 & 0 & 0\\ 0 & 0 & 0 & 0 & (1-2\nu)/2 & 0\\ 0 & 0 & 0 & 0 & 0 & (1-2\nu)/2\end{bmatrix}\begin{bmatrix}\varepsilon_1\\ \varepsilon_2\\ \varepsilon_3\\ 2\varepsilon_4\\ 2\varepsilon_5\\ 2\varepsilon_6\end{bmatrix} \tag{18}$$

where E and ν are Young's modulus and Poisson's ratio, respectively.

Combining equation (18) and equations (15)–(17), the relationship between the linear stiffness coefficients of the bonds and the macroscopic material constants can be established. However, the four spring stiffness cannot be uniquely determined because there are only three equations of equilibrium. To solve this over-determined problem, the shear stiffness $k_{\mathrm{s}}^{\mathrm{p}}$ of bond B_1 in principal directions is assumed to be zero, since the shear stiffness $k_{\mathrm{s}}^{\mathrm{o}}$ has components in principal directions and the contribution of $k_{\mathrm{s}}^{\mathrm{p}}$ to macroscopic elasticity can be represented in terms of $k_{\mathrm{s}}^{\mathrm{o}}$, as seen in equation (13). Thus, the other spring constants $k_{\mathrm{n}}^{\mathrm{p}}$, $k_{\mathrm{n}}^{\mathrm{o}}$ and $k_{\mathrm{s}}^{\mathrm{o}}$ can be determined as follows

$$\begin{aligned} k_{\mathrm{n}}^{\mathrm{p}} &= \frac{EL}{4(1+\nu)(1-2\nu)}\\ k_{\mathrm{n}}^{\mathrm{o}} &= \frac{(1+2\nu)EL}{4(1+\nu)(1-2\nu)}\\ k_{\mathrm{s}}^{\mathrm{o}} &= \frac{(1-4\nu)EL}{4(1+\nu)(1-2\nu)} \end{aligned} \tag{19}$$

It can be seen that the shear stiffness $k_{\mathrm{s}}^{\mathrm{o}}$ will become negative when the Poisson's ratio ν exceeds 1/4. This indicates that the physical Poisson's ratio range resulting from the site-bond model is $-1 < \nu \le 1/4$, since the negative spring constant seems non-physical. However, it is proved by molecular dynamics simulations that the negative stiffness still has a physical explanation at the molecular level.[10] Therefore, the shear spring with negative stiffness can be added in order to model a material with a Poisson's ratio higher than 1/4 but lower than 1/2.

Benchmark tests

Numerical benchmark tests are carried to validate the derived spring stiffness coefficients. The macroscopic Young's modulus and Poisson's ratio are selected as E=11 000 MPa and ν=0·2. The stiffness coefficients of springs are calculated from equation (19). A cubic site-bond arrangement with size of $10L$ by $10L$ by $10L$ is used for simulations. This means that there are 10 unit cells in each principal direction; illustration given in Fig. 2. The assembly is subjected to various loading conditions, i.e. uniaxial tension and plane strain, to estimate the macroscopic Young's modulus, Poisson's ratio and modulus of rigidity independently.

For uniaxial tension, the sites X_1=0, X_2=0 and X_3=0 are fixed in the X_1, X_2 and X_3 direction, respectively. A displacement of L in the X_3 direction is applied at sites X_3=$10L$ and other sites are free, which induces a macroscopic tensile strain $\varepsilon_{\mathrm{t}} = \varepsilon_3 = L/10L = 0{\cdot}1$. The macroscopic Poisson's ratio ν for tension and compression is calculated according to $\nu = -\varepsilon_1/\varepsilon_3$ or $\nu = -\varepsilon_2/\varepsilon_3$, in which $\varepsilon_1 = u_1/10L$ and $\varepsilon_2 = u_2/10L$ are identical. Here,

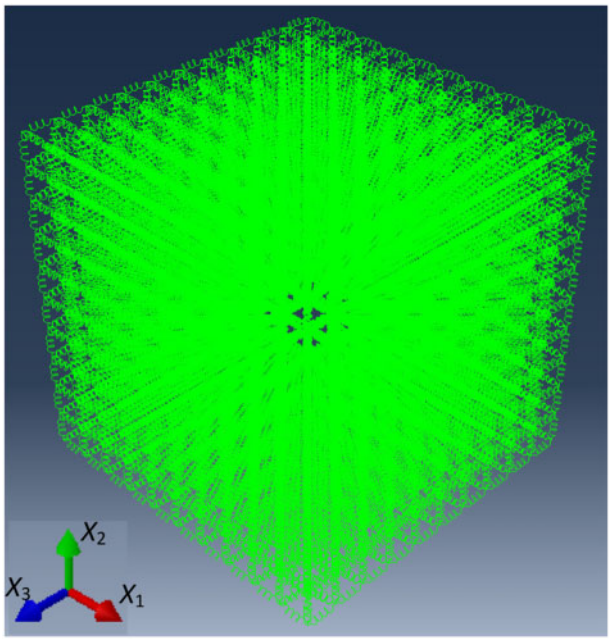

2 Generated lattice $10L \times 10L \times 10L$

u_1 and u_2 stand for the average displacements in the X_1 and X_2 directions of sites on plane $X_1=10L$ and $X_2=10L$, respectively. The macroscopic modulus of elasticity is estimated using $E=\sigma_t/\varepsilon_t$, where the macroscopic stress in the X_3-direction σ_t is computed by $\sigma_t=f_3/(10L\cdot 10L)$ and f_3 is the reaction force at sites on plane $X_3=0$. Figure 3 demonstrates the contour plot of the simulated von Mises stress by site-bond model under uniaxial tensile loading. The calculated macroscopic elastic modulus E is 11 225 and Poisson's ratio ν is 0·1973, which have a relative error of about 2·05 and 1·35%, respectively, compared to the imposed values. This shows that the proposed site-bond model is capable of simulating the elasticity of solids under uniaxial tension with a very good accuracy.

With respect to plane strain tension test, the sites on both $X_1=0$ and $X_1=10L$ are fixed in the X_1 direction.

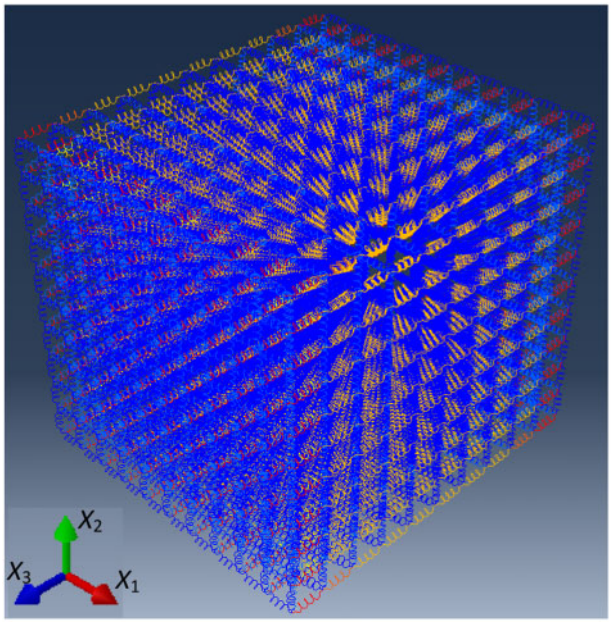

3 Simulated von Mises stress under uniaxial tension

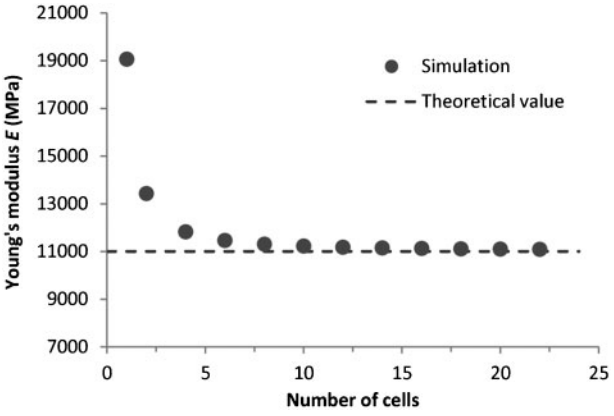

4 Predicted Young's modulus against number of cells in principal direction

The sites on $X_2=0$ are fixed in the X_2 direction. The sites on $X_3=0$ are fixed in the X_3 direction. The displacements of L in the X_2 and X_3 directions are imposed at sites $X_2=10L$ and $X_3=10L$, respectively. The other sites are free. Thus, two macroscopic tensile strains $\varepsilon_2=L/10L=0{\cdot}1$ and $\varepsilon_3=L/10L=0{\cdot}1$ are imposed on the lattice and the strain in the X_1 direction is zero. The macroscopic modulus of rigidity can be computed according to $G=[\sigma_3-\lambda(\varepsilon_1+\varepsilon_2+\varepsilon_3)]/2\varepsilon_3$, in which the macroscopic stress in the X_3 direction σ_3 is calculated using $\sigma_3=f_3/(10L\cdot 10L)$ and f_3 is the measured reaction force at sites on plane $X_3=0$. The Lamé's first parameter is calculated by $\lambda=Ev/[(1+v)(1-2v)]$. The Poisson's ratio and Young's modulus are obtained as $v=\sigma_1/(\sigma_2+\sigma_3)$ and $E=(\sigma_3-v(\sigma_1+\sigma_2))/\varepsilon_3$. It is found that the Young's modulus and Poisson's ratio obtained from plane strain tension test are the same as those derived from uniaxial tension test. The calculated shear modulus according to the method as introduced beforehand is 4691, which has a 2·35% difference relative to the theoretical value of $G=11000/[2(1+0{\cdot}2)]=4583{\cdot}33$ MPa. This means that the site-bond model with the derived normal and shear spring constants is able to simulate the elastic behaviour of an isotropic material under shear loading.

To investigate the influence of the number of unit cells on the estimated macroscopic elastic constants, a set of cubic cellular lattices with various sizes from L^3 to $10\,648L^3$ is generated. Simulations are performed with

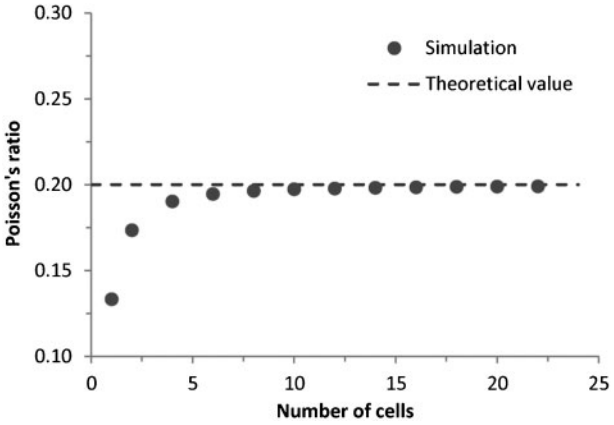

5 Predicted Poisson's ratio against number of cells in principal direction

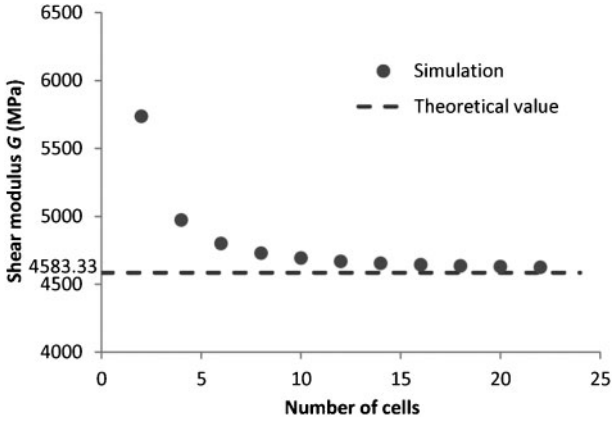

6 Predicted shear modulus against number of cells in principal direction

the plane strain boundary conditions. The predicted macroscopic Young's modulus, Poisson's ratio and shear modulus against the number of unit cells in each principal direction of a cubic region are plotted in Figs. 4–6.

It can be seen that the simulated macroscopic Young's modulus and shear modulus decrease with the increase in the number of cells in principal direction. On the contrary, the estimated Poisson's ratio increases with the increasing size of cellular lattice. Eventually, the simulated elastic constants tend to their corresponding theoretical values with the increase in the size of cellular lattice. This is attributed to the smaller boundary effect when the size of region is larger. When the number of cells in principal direction is higher than 20, the estimated results are close enough to the theoretical values.

The generated site-bond model can be considered as a valid representation of isotropic elastic material. Based on the definition of criterion for bond failure and relevant implementation as presented in a previous study by Jivkov *et al.*,[6] the fracture process and damage evolution in quasi-brittle materials can be simulated by using the proposed site-bond model. This is a subject of ongoing work. In addition, the effects of microstructure parameters, such as porosity, pore size distribution and connectivity of solid phase, on the macroscopic behaviour, stress–strain response of quasi-brittle materials will be investigated. The results of these aspects will be reported in future publications.

Conclusion

This work presents a meso-scale model for macroscopic elasticity of solids. The model is based on a cellular lattice of truncated octahedrons, filling the space compactly. The cellular architecture is transformed into discrete site-bond lattice with bonds containing normal and shear springs. The spring stiffness coefficients are obtained as functions of macroscopic elastic constants. From the findings of the present study, the following conclusions can be drawn.

1. The site-bond assembly represents generally a macroscopic cubic elasticity and is able to deliver any macroscopic isotropic elasticity.
2. The physical Poisson's ratio range results from the site-bond model is $-1<\nu<1/2$.
3. For uniaxial tension test, the estimated macroscopic Young's modulus and Poisson's ratio show a very good agreement with the theoretical ones.
4. For plane strain test, the measured macroscopic modulus of rigidity fit very well with the theoretical value.
5. The size of cellular lattice plays an important role in the accuracy of simulation due to boundary effect. When the number of cells in principal direction is higher than 20, the obtained simulation results are close enough to the theoretical data.
6. The proposed site-bond model is regarded as a very good representation of isotropic elastic materials, and will be applied to simulate the fracture process and damage evolution in quasi-brittle materials.

Acknowledgements

M. Zhang and A. P. Jivkov acknowledge the support from EPSRC via grant no. EP/J019763/1, 'QUBE: Quasi-Brittle fracture: a 3D experimentally-validated approach', and from BNFL for the Research Centre for Radwaste & Decommissioning. C. N. Morrison greatly appreciates the support from EPSRC via Nuclear FiRST Doctoral Training Centre.

References

1. A. P. Jivkov and J. R. Yates: 'Elastic behaviour of a regular lattice for meso-scale modelling of solids', *Int. J. Solids. Struct.*, 2012, **49**, 3089–3099.
2. E. Schlangen and J. G. M. van Mier: 'Experimental and numerical analysis of micromechanisms of fracture of cement-based composites', *Cem. Concr. Compos.*, 1992, **14**, 105–118.
3. C. S. Chang, T. K. Wang, L. J. Sluys and J. G. M. van Mier: 'Fracture modelling using a micro structural mechanics approach. I: Theory and formation', *Eng. Fract. Mech.*, 2002, **69**, 1941–1958.
4. D. V. Griffiths and G. G. W. Mustoe: 'Modelling of elastic continua using a grillage of structural elements based on discrete element concepts', *Int. J. Numer. Meth. Eng.*, 2001, **50**, 1759–1775.
5. E. Schlangen: 'Crack development in concrete. Part 2: Modelling of fracture process', *Key Eng. Mater.*, 2008, **73–76**, 385–387.
6. A. P. Jivkov, D. L. Engelberg, R. Stein and M. Petkovski: 'Pore space and brittle damage evolution in concrete', *Eng. Fract. Mech.*, 2013, **110**, 378–395.
7. Y. Wang and P. Mora: 'Macroscopic elastic properties of regular lattices', *J. Mech. Phys. Solids*, 2008, **56**, 3459–3474.
8. M. Ostoja-Starzewski: 'Lattice models in micromechanics', *Appl. Mech. Rev.*, 2002, **55**, 35–60.
9. G. Wang, A. Al-Ostaz, A. H.-D. Cheng and P. R. Mantena: 'Hybrid lattice particle modelling: Theoretical considerations for a 2D elastic spring network for dynamic fracture simulations', *Comput. Mater. Sci.*, 2009, **44**, 1126–1134.
10. S. Zhao and G. Zhao: 'Implementation of a high order lattice spring model for elasticity', *Int. J. Solids. Struct.*, 2012, **49**, 2568–2581.